Nanoscale

Ultrafine CoO nanoparticles as an efficient cocatalyst for enhanced photocatalytic hydrogen evolution

Journal:	*Nanoscale*
Manuscript ID	NR-ART-06-2019-005086.R1
Article Type:	Paper
Date Submitted by the Author:	20-Jul-2019
Complete List of Authors:	Chu, Jiayu; Harbin Institute of Technology, Department of Chemistry Sun, Guoji; Harbin Institute of Technology Shenzhen Graduate School, State Key Laboratory of Advanced Welding and Joining Han, Xijiang; Harbin Institute of Technology Chen, Xin; Peking University,Shool of Advanced Materials, Wang, Jiajun; Harbin Institute of Technology, School of Chemistry and Chemical Engineering Hu, Wen; Brookhaven National Laboratory Waluyo, Iradwikanari; Brookhaven National Laboratory, National Synchrotron Light Source II Hunt, Adrian; North Carolina State University, Physics Du, Yunchen; Harbin Institute of Technology, School of Chemistry and Chemical Engineering Song, Bo; Harbin Istitute of Technology, 2Academy of Fundamental and Interdisciplinary Sciences Xu, Ping; Harbin Institute of Technology, School of Chemistry and Chemical Engineering

ARTICLE

Ultrafine CoO nanoparticles as an efficient cocatalyst for enhanced photocatalytic hydrogen evolution

Received 00th January 20xx,
Accepted 00th January 20xx

DOI: 10.1039/x0xx00000x

Jiayu Chu,[a] Guoji Sun,[b] Xijiang Han,*[a] Xin Chen,[c] Jiajun Wang,[a] Wen Hu,[d] Iradwikanari Waluyo,[d] Adrian Hunt,[d] Yunchen Du,[a] Bo Song,*[e] and Ping Xu*[a]

In order to further enhance the performance of photocatalysts, cocatalysts are applied to accelerate the photocatalytic reactions. Herein, ultrafine cobalt oxide (CoO) nanoparticles are synthesized through a novel bottom-up strategy and explored as an efficient non-noble cocatalyst to dramatically promote the photocatalytic hydrogen evolution rate of CdS nanorods. CdS/CoO heterostructures, consisting of highly dispersed 3-5 nm CoO nanoparticles anchored on the CdS nanorods, can provide a high photocatalytic hydrogen evolution rate of 6.45 mmol g^{-1} h^{-1} (~36 times higher than that of bare CdS nanorods) in the visible-light region (>420 nm). Combined X-ray photoelectron spectroscopy and X-ray absorption near edge spectroscopy analyses suggest Co-S bond formation between CoO and CdS, which guarantees efficient migration and separation of photogenerated charge carriers. This work provides a new avenue for adopting CoO as an effective cocatalyst for enhanced photocatalytic hydrogen production in the visible-light region.

Introduction

Overcoming the issues of environmental pollution and energy shortage is the most urgent challenge to human society.[1-4] Hydrogen, as a clean energy source, has attracted tremendous attention to solve this thorny problem.[5-7] Among the various hydrogen-generation technologies, photocatalytic hydrogen evolution has always been a promising route for water splitting because of the inexhaustible advantage of solar energy.[8-12] However, the high recombination rate of photogenerated charge carriers remains an intractable issue for most photocatalysts. With this regard, introduction of cocatalysts becomes an effective approach to suppressing the electron-hole recombination, lowering the overpotential for hydrogen production as well as enhancing the light absorption.[13-16] In recent decades, various cocatalysts, such as noble metals (Pt,[17] Pd,[18] Rh[19]), non-noble metals (Ni,[13] Cu[20]), or metal sulfides (MoS_2,[21] NiS[22, 23]), have been developed as cocatalysts in photocatalytic hydrogen evolution. However, noble metal cocatalysts, with remarkable performance, are limited by their high cost and scarcity.[24] While, for non-noble cocatalysts, their performance are still not comparable to that of Pt or other noble metal cocatalysts.[25] Therefore, it is urgent to develop highly active and cost-effective cocatalysts as alternatives to noble metal ones.

Cobalt (II) oxide (CoO) has a promising optical response toward the visible light and strong electron transport properties due to its merits of a relatively narrow bandgap (2.6 eV).[26, 27] Recently, CoO has gained increasing attention since Bao et al. firstly reported that CoO could decompose pure water under visible-light irradiation.[28] CoO/g-C_3N_4 heterojunctions with CoO nanoparticles uniformly dispersed on the g-C_3N_4 surface displayed enhanced photocatalytic activity and stability, and in this case CoO plays the role of reduction center for hydrogen evolution due to a higher conduction band (CB) of g-C_3N_4 than that of CoO.[29] Nevertheless, to date, only a few studies have focused on CoO as a candidate in photocatalytic hydrogen evolution and the rate of hydrogen evolution remains relatively low.[27, 29-31] Also, there is a fatal flaw that aggregated CoO nanoparticles have almost no photocatalytic activity,[29] and thus synthesis strategy of highly dispersed CoO nanoparticles is highly demanded.

Herein, a bottom-up pathway is developed for fabricating CdS/CoO heterostructures with highly dispersed ultrafine CoO nanoparticles on the surface of CdS nanorods (Scheme 1). The as-prepared ultrafine CoO nanoparticles, as a novel and efficient cocatalyst, can significantly enhance the photocatalytic hydrogen evolution rate of CdS nanorods. The highly dispersed CoO nanoparticles are obtained through a modified procedure in preparing ZIF-67 metal organic frameworks (MOFs). It should be pointed out that CdS nanorods were wrapped by hierarchical ultrathin amorphous $Co(OH)_2$ nanosheets when we increased

[a] *MIIT Key Laboratory of Critical Materials Technology for New Energy Conversion and Storage, School of Chemistry and Chemical Engineering, Harbin Institute of Technology, Harbin 150001, China. Email: pxu@hit.edu.cn (P.X.).*
[b] *State Key Laboratory of Advanced Welding and Joining, Harbin Institute of Technology, Shenzhen Graduate School, Shenzhen 518055, China.*
[c] *School of Advanced Materials, Peking University, Shenzhen Graduate School, Shenzhen 518055, China.*
[d] *National Synchrotron Light Source II, Brookhaven National Laboratory, Upton, NY 11973, USA.*
[e] *Academy of Fundamental and Interdisciplinary Sciences, Harbin Institute of Technology, Harbin 150001, China. Email: songbo@hit.edu.cn (B.S.).*
Electronic Supplementary Information (ESI) available: Figure S1-S25, and Table S1-S3. See DOI: 10.1039/x0xx00000x

the relative ratio of Co^{2+} ions to 2-methylimidazole (2MIM) in an original attempt to synthesize ZIF-67 on CdS nanorods (see Experimental Section for details), which however provides a unique opportunity to fabricate ultrafine CoO nanoparticles decorated on CdS nanorods (termed as CdS/CoO heterostructures) through a subsequent calcination process under mild conditions.

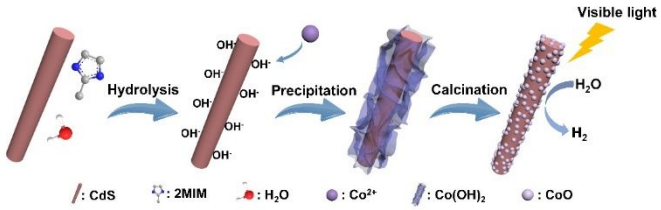

Scheme 1 Schematic illustration of preparing CdS/CoO heterostructures. Hydrolysis of 2MIM in the presence of water produces a strong local alkaline environments at the CdS surface, and hierarchical $Co(OH)_2$ nanosheets can be produced with the addition of Co^{2+} ions. Subsequent calcination of the CdS/$Co(OH)_2$ nanocomposites leads to ultrafine CoO nanoparticles uniformly decorated on the CdS nanorods.

Experiment Section

Synthesis of CdS nanorods. CdS nanorods were fabricated through our previous method.[32] Briefly, 1.87 g of $Cd(NO_3)_2{\cdot}4H_2O$ and 1.38 g of NH_2CSNH_2 were ultrasonically dispersed into 30 mL of ethylenediamine, and then the solution was transferred into a Teflon liner and maintained at 160 °C for 24 h. After that, the obtained yellow precipitates were centrifuged, rinsed with distilled water and ethanol for several times, and then dried in a vacuum drier at 60 °C for further use.

Synthesis of CdS/$Co(OH)_2$ nanocomposites. CdS/$Co(OH)_2$ was prepared through a modified procedure in attempt to grow ZIF-67 on CdS nanorods. Typically, 50 mg of CdS nanorods were dispersed into 100 mL of methanol containing 0.82 g of 2-methylimidazole. After being ultrasonically treated for 2 h, 100 mL of methanol containing 2.91 g of $Co(NO_3)_2{\cdot}6H_2O$ were added into the above solution and stirred for different time periods (0.25 , 1 , 3 and 6 h). The product was washed with methanol for three times and dried in a vacuum drier at 60 °C.

Synthesis of CdS/CoO heterostructures. The obtained CdS/$Co(OH)_2$ nanocomposites were calcined in a tube furnace at 600°C for 2 h at a rate of 2 °C min^{-1} under a continuous flow of Ar. The final samples were denoted as CdS/CoO-*x* heterostructures, where *x* represents the reaction time during the preparation of CdS/$Co(OH)_2$ nanocomposites precursors.

Characterization . Scanning electron microscopy (SEM) images were obtained on HELIOS NanoLab 600i (FEI Instruments). Transmission electron microscopy (TEM) images were obtained on Tecnai F20 (FEI Instruments) at an accelerating voltage of 200 kV. Powder X-ray diffraction (XRD) data were recorded on a Rigaku D/Max-RC X-ray diffractometer with Cu Kα radiation source (45.0 kV, 50.0 mA). X-ray photoelectron spectroscopy (XPS) was performed on a PHI-5400 ESCA system using an Al Kα radiation as a source. The binding energy was calibrated using the C 1s photoelectron peak at 284.6 eV as reference. Inductively coupled plasma-atomic emission spectrometry (ICP−AES) was measured on PerkinElmer (PE) Optima 8300. The UV−vis absorption spectra were collected on a Hitachi UH4150 spectrometer. Photoluminescence (PL) spectra were recorded on a PerkinElmer LS 55 spectrometer in the wavelength range of 450−800 nm, using an excitation wavelength of 450 nm. Nitrogen adsorption/desorption isotherms were collected on QUADRASORB SI-KR/MP (Quantachrome, USA) after heating the materials in vacuum for 2 h at 120 °C. Soft X-ray absorption spectroscopy measurements were performed at the 23-ID-2 (IOS) beamline at the National Synchrotron Light Source II (NSLS-II), Brookhaven National Laboratory. Co L-edge XANES spectra were acquired in the total electron yield (TEY) mode through drain current measurements. The samples were mounted on an indium foil on a sample holder prior to introduction into the ultra-high vacuum chamber. The spectra were normalized to the current on a gold mesh located upstream of the sample.

Mott-Schottky measurement. Mott-Schottky analysis was applied to calculate and compare the density of charge carriers (N_d) of the photocatalysts, providing further insight into the process of photocatalytic hydrogen evolution. The carrier density is calculated by eq 1:[33]

$$N_{\mathrm{d}} = \frac{2/e_0\varepsilon\varepsilon_0}{\mathrm{d}\left(1/C^2\right)/\mathrm{d}V} \quad (1)$$

where e_0 is the electron charge, ε is the dielectric constant of the semiconductor, ε_0 is the permittivity of vacuum, C is the capacitance, and V is the applied bias at the electrode. Here, we take ε=11.6 for CdS.

Photocatalytic hydrogen evolution test. The photocatalytic reactions were conducted on a vacuum-closed gas-circulation system with a top window at room temperature, which was sealed with a silicone rubber septum. A 300 W Xe lamp (PLS-SXE300/300UV) with a cut off filter (>420 nm) was employed, which was positioned 10 cm away from the reactor, and the intensity focused on the reaction system was measured to be ~180 mW cm^{-2}. In a typical procedure, 50 mg of the as-prepared catalyst was dispersed into 100 mL aqueous solution containing 20 mL of lactic acid. Prior to irradiation, the reaction system was pumped to vacuum for 45 min. The amount of produced H_2 was measured by gas chromatography (Techcomp GC7900) with a thermal conductivity detector (TCD), with N_2 as the carrier gas. Here, no noble metal co-catalyst (H_2PtCl_6) was added into the reaction system.

The apparent quantum yield (AQY) for hydrogen evolution at the fixed wavelength of 420 and 500 nm are calculated according to eq 2:[2]

$$\mathrm{AQY}=\frac{N_{\mathrm{e}}}{N_{\mathrm{p}}}\times 100\% = \frac{2MN_{\mathrm{A}}hc}{SPt\lambda}\times 100\% \quad (2)$$

where N_e is the amount of reaction electrons, N_p is the amount of incident photons, M is the amount of H_2 molecules, N_A is Avogadro's number, h is Planck's constant, c is the speed of light, S is the irradiation area, P is the intensity of the irradiation light, t is the reaction time, and λ is the wavelength of the incident light (420 and 500 nm).

Photoelectrochemical test. The photoelectrochemical measurements were carried out using a standard three-electrode

cell on a CHI 660D (CH Instruments, Inc.) electrochemical workstation, with a Ag/AgCl reference electrode, a platinum foil as a counter electrode and the as-prepared photocatalyst film electrodes on FTO glass as the working electrode. The photoanodes were prepared by a spray coating method, using a glass-rod to roll a paste containing 30 mg of powders and 2 mL of EtOH on a transparent FTO glass-substrate, followed by calcining for 120 min at 400 °C under a N_2 atmosphere with a heating rate of 5 °C min^{-1}. KOH (0.1 M) was purged with N_2 and used as the electrolyte. Electrochemical impedance spectroscopy was measured at the potential of 0.6 V vs Ag/AgCl.

Computational methods. All calculations were performed using the density functional theory (DFT) by the Vienna *Ab-initio* Simulation Package (VASP).[34] The interactions between valence electrons and ions were treated with the projector augmented wave (PAW) potentials.[35] The exchange-correlation interactions were described by generalized gradient approximation (GGA)[36] with the Perdew-Burke-Ernzerhof (PBE) functional.[36] Spin-polarization was included through all the calculations, an effective U-J parameter of 3.7 was applied to improve the description Co 3d states.[37] The electron wave functions were expanded in a plane-wave basis with a cut-off energy of 520 eV. The convergence criteria for residual force and energy on each atom during structure relaxation were set to 0.01 eV A^{-1} and 10^{-3} eV, respectively. The vacuum space was more than 15 Å to avoid the interaction between periodical images. The Brillouin zone was sampled with the Monkhorst−Pack mesh with a K-point of 4 × 4 × 1 grid in reciprocal space.

In the above system, the hydrogen adsorption free energy ΔG_H can be calculated by eq 3:

$$\Delta G_H = \Delta E_H + \Delta ZPE + T\Delta S_H \quad (3)$$

where ΔE_H represents the adsorption energy of one hydrogen atom, which is calculated according to eq 4, ΔZPE denotes the zero point energy difference between the adsorbed state of the system and the gas phase state obtained by $hv/2$. $T\Delta S_H$ is the gas-phase entropy contribution of a hydrogen molecule and can be calculated by eq 5.

$$\Delta E_H = E(H^*) - E(^*) - 1/2E(H_2) \quad (4)$$

$$\Delta S_H \cong -\frac{1}{2} S^0_{H_2} \quad (5)$$

where * refers to the catalyst used for hydrogen evolution, $E(^*)$ and $E(H^*)$ are the total energies of the surface system and the surface system with one adsorbed H, respectively. $E(H_2)$ represents the total energy of a gas phase H_2 molecule, and $\boldsymbol{S^0_{H_2}}$ is the entropy of H_2 in gas phase at the standard condition.

Results and Discussion

The formation of amorphous $Co(OH)_2$ can be verified by combined X-ray diffraction (XRD) (Fig. S1 in ESI†) and Raman studies (Fig. S2 in ESI†) in the CdS/$Co(OH)_2$ nanocomposites. The morphology evolution from CdS nanorods to CdS/$Co(OH)_2$ nanocomposites and then to CdS/CoO heterostructures were investigated by scanning electron microscopy (SEM) and transmission electron microscopy (TEM). As-prepared CdS nanorods are highly uniform with an average diameter of about 50-80 nm and smooth surface (Fig. S3 in ESI†), which can be fully wrapped by the soft and wrinkled $Co(OH)_2$ nanosheets under proper reaction conditions (Fig. 1a). The content of $Co(OH)_2$ nanosheets on the CdS nanorods can be effectively tuned by controlling the reaction time (Fig. S4 in ESI†). Notably, TEM image reveals that the $Co(OH)_2$ nanosheets are ultrathin and closely packed on the surface of CdS nanorods (Fig. 1b). High resolution TEM (HRTEM) observation (Fig. S5 in ESI†) confirms the amorphous nature of the $Co(OH)_2$ nanosheets. After calcination, ultrafine CoO nanoparticles converted from the $Co(OH)_2$ nanosheets are uniformly grown on the CdS nanorods (Fig. 1c and 1d). Similarly, the loading amount and size of CoO nanoparticles in the CdS/CoO heterostructures can also be manipulated from the CdS/$Co(OH)_2$ precursors (Fig. S6 in ESI†). Meanwhile, the molar ratios of Co to Cd in CdS/CoO-*x* heterostructures (*x* represents the reaction time during preparing CdS/$Co(OH)_2$ nanocomposites) were determined by X-ray photoelectron spectroscopy (XPS) and Inductively coupled plasma-atomic emission spectrometry (ICP−AES) techniques (Table S1 in ESI†), which suggest more CoO loaded on CdS with prolonged reaction time. Taking CdS/CoO-1h for example, the size of CoO nanoparticles is about 3-5 nm (red areas in Fig. 1e). HRTEM image and selected area electron diffraction (SAED) pattern in Fig. 1f clearly display the lattice spacing of 0.358 and 0.246 nm that can be assigned to the (100) plane of hexagonal CdS and (111) plane of cubic CoO, respectively. Elemental mapping from the high-angle annular dark-field scanning TEM (HAADF-STEM) image (Fig. 1g) shows that Cd, S, Co and O elements are homogeneously distributed over the nanorods, another proof of the successful fabrication of CoO nanoparticles uniformly decorated on the CdS nanorods without obvious aggregation in the CdS/CoO heterostructures.

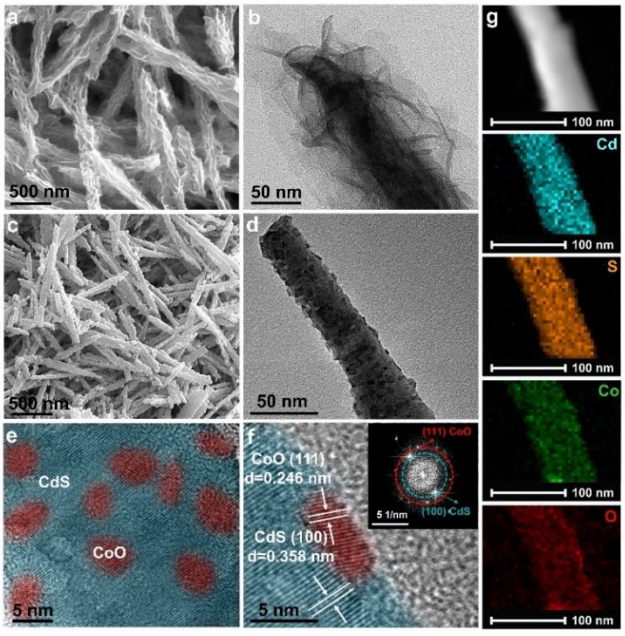

Fig. 1 (a) SEM image and (b) TEM image of CdS/$Co(OH)_2$ nanocomposites, (c) SEM image, (d) TEM image, (e, f) HRTEM and fast Fourier transform (FFT) image of CdS/CoO-1h heterostructures, (g) HAADF-STEM image and EDS mapping of a single CdS/CoO-1h heterostructure.

One may wonder how is $Co(OH)_2$ formed? It is worth noting that CdS/ZIF-67 (Fig. S7 in ESI†) can be obtained when the molar ratio of Co^{2+} ions to 2MIM is ~1:7, which is the ratio usually used for preparing MOFs materials.[38] Interestingly, when the ratio is ~1:1.4, a critical structure containing both ZIF-67 and $Co(OH)_2$ nanosheets can be obtained (Fig. S8 in ESI†). CdS nanorods fully wrapped by $Co(OH)_2$ nanosheets can be prepared when the ratio is greater than 1:1.4. Our control experiments strongly suggest a hydrolysis-precipitation process: when the CdS nanorods are dispersed into the methanol solution containing 2MIM, a local alkaline environment on the surface of the CdS nanorods is formed by hydrolyzing 2MIM with the water present in methanol. Subsequent addition of Co^{2+} ions promotes the growth of $Co(OH)_2$ nanosheets at the CdS surface. If the adding order of Co^{2+} ions and 2MIM is reversed, very limited $Co(OH)_2$ nanosheets can be observed (Fig. S9 in ESI†), indicating the important role of local alkaline environment at CdS surface. In order to verify the hydrolysis process of 2MIM, we removed water in methanol by method of reflux with magnesium rod and keeping $Co(NO_3)_2{\cdot}6H_2O$ and 2MIM in a vacuum drier for 24 h. As expected, no $Co(OH)_2$ nanosheets are found on the surface of CdS nanorods (Fig. S10 in ESI†). Notably, addition of some water purposely into the above anhydrous system leads to similar $Co(OH)_2$ nanosheets again (Fig. S11 in ESI†). These results convincingly reveal that the trace water in methanol will lead to the hydrolysis of 2MIM and thus generate a local strong alkaline environment for the precipitation of Co^{2+} ions into ultrathin $Co(OH)_2$ nanosheets. Of particular interest is that no precipitation can be found when the solution only contains Co^{2+} ions and 2MIM at a molar ratio of 1:1.4 (without CdS nanorods) even after 48 h, an indication that CdS nanorods are also crucial for forming a local alkaline environment at their surface for the growth of $Co(OH)_2$ nanosheets. However, when there is a large amount of OH^- in the system (the reaction solvent is only water), heavily aggregated $Co(OH)_2$ nanoparticles will be obtained quickly (Fig. S12 in ESI†). Above results confirm that CdS nanorods and trace water are indispensable for the formation of CdS nanorods uniformly wrapped by ultrathin $Co(OH)_2$ nanosheets. What's more, this method is also suitable for the acquisition of other materials that are wrapped by hierarchical $Co(OH)_2$ nanosheets, such as $TiO_2/Co(OH)_2$ and $Cu_2O/Co(OH)_2$ (Fig. S13 in ESI†), which might become a novel and general route for the fabrication of $Co(OH)_2$ nanosheets on other supports.

The crystal structure and composition of the prepared samples were characterized by X-ray diffraction (XRD) in Fig. 2a. XRD pattern of CdS nanorods corresponds to standard hexagonal phase (JCPDS No.41-1049). The peaks ascribed to the $Co(OH)_2$ nanosheets in the CdS/$Co(OH)_2$ nanocomposites could not be found, due to their amorphous feature. For the CdS/CoO-1h heterostructures, the diffraction peaks at 2ϑ= 36.5, 42.4, 61.5, 73.7 and 77.6° can be indexed to the (111), (200), (220), (311) and (222) planes of cubic CoO (JCPDS No.43-1004). In addition, the presence of CoO can also be verified by the Raman bands at 485, 530 and 690 cm^{-1} (Fig. S2 in ESI†).[39, 40] In order to understand the interaction between CoO and CdS in the CdS/CoO heterostructures, XPS spectra of CdS, CoO and CdS/CoO-1h heterostructures were compared (Fig. 2b, 2c and S14 in ESI†). For Co 2p level (Fig. 2b), the peaks at 778.2 and 793.7 eV can be ascribed to Co $2p_{3/2}$ and Co $2p_{1/2}$ of Co-S bonds.[27, 40-42] Meanwhile, besides the features of S in CdS, the characteristic peaks located at 161.7 and 162.8 eV in the S 2p spectrum agree well with S $2p_{3/2}$ and S $2p_{1/2}$ of Co-S bonds (Fig. 2c).[40] Above results confirm that CoO nanoparticles are bonded on the surface of CdS nanorods through the formation of Co-S bonds. Further observation of the peaks of Co-O bonds reveals that the Co 2p peaks in the CdS/CoO-1h heterostructures shift to a higher energy position as compared to those of CoO. Similarly, in the S 2p and Cd 3d spectra (Fig. S15 in ESI†), the peaks of Cd-S bonds move to lower energy positions, which further reveals that the electron density of CdS is increased with the decoration of CoO nanoparticles.[32, 43-46] Moreover, the Co L-edge X-ray absorption near edge spectroscopy (XANES) also shows a similar energy shift phenomenon (Fig. 2d), where two main peaks (L_{II} and L_{III}) are presented due to core-level spin-orbit coupling and further splitting at L_{III} peak is due to the multiple structure from electron-electron interactions that can imply the local symmetry.[47, 48] Apparently, the Co atoms of typical CoO are octahedrally coordinated (O_h), and some feature of tetrahedrally coordinated (T_d) structure appears once CoO is anchored on the CdS nanorods due to the formation of Co-S bonds. Above results confirm that CoO and CdS are interconnected through the Co-S bonds in the CdS/CoO heterostructures.

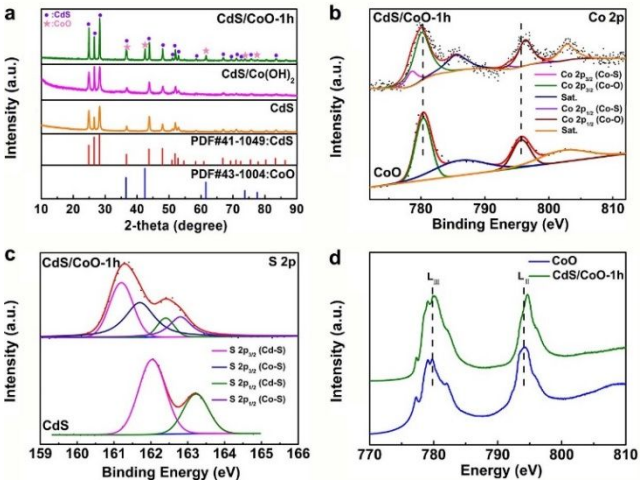

Fig. 2 (a) XRD patterns of CdS, CdS/$Co(OH)_2$ nanocomposites and CdS/CoO-1h heterostructures, (b) high-resolution XPS spectrum of Co 2p of CoO nanoparticles and CdS/CoO-1h heterostructures, (c) high-resolution XPS spectrum of S 2p of CdS nanorods and CdS/CoO-1h heterostructures, (d) Co $L_{II,III}$-edge X-ray absorption near edge spectra of the CoO nanoparticles and CdS/CoO-1h heterostructures.

To acquire insight into the photocatalytic response, spectroscopic and photochemical studies were conducted. The UV-vis absorption spectra of the photocatalysts are essential to measure their light-harvesting abilities. As shown in Fig. 3a, the CdS/CoO-1h heterostructures exhibit much enhanced absorption than CdS nanorods in the visible light region due to

the presence of CoO. It is worth noting that the absorption features vary with the CoO content in the CdS/CoO heterostructures (Fig. S16 in ESI†), indicating that the light absorption capacity can be adjusted by the amount of CoO. Here, the light absorption in the visible region increases from CdS/CoO-0.25h to CdS/CoO-1h, and then gets decreased for CdS/CoO-3h and CdS/CoO-6h, suggesting that too much loading of CoO will, on the contrary, hinder the light absorption of CdS in the CdS/CoO heterostructures. In addition, the light harvesting efficiency (LHE) of the CdS and CdS/CoO-1h (Fig. S17 in ESI†) were calculated from the measured reflection (R) and transmission (T) according to LHE (λ) (%) = 100% - $R(\lambda)$ (%) - $T(\lambda)$ (%).[49] It is shown that the LHE of CdS/CoO-1h heterostructures is much higher than that of CdS in the visible light region because of the existence of CoO. The bandgap of CdS/CoO heterostructures is calculated to be about 2.24 eV (Fig. 3b), narrower than that of CdS nanorods (2.41 eV), which may substantially enhance the photocatalytic activity due to the broadened light harvesting.

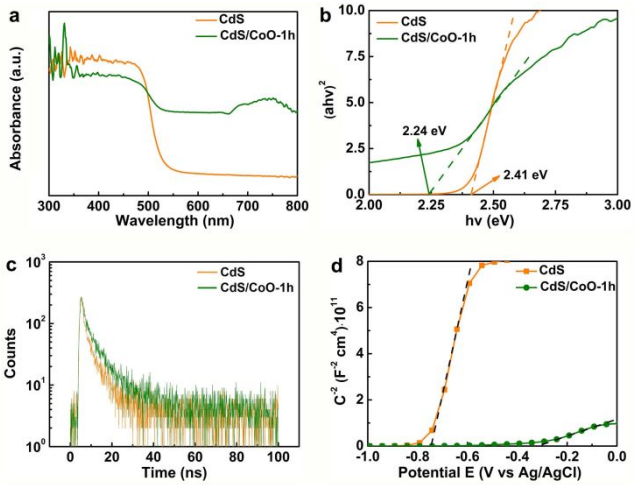

Fig. 3 (a) UV-vis absorption spectra, (b) optical bandgaps, (c) Time-resolved transient PL decay and (d) Mott-Schottky plots of the CdS nanorods and CdS/CoO-1h heterostructures.

Meanwhile, the behavior of charge trapping and separation in the CdS and CdS/CoO heterostructures was compared by the photoluminescence (PL) spectra (Fig. S18 in ESI†). The original CdS nanorods show a strong emission peak at ~575 nm, which is derived from the inter-band recombination of electron and holes. While the PL emission intensity of CdS/CoO-1h heterostructures is dramatically decreased as compared to that of CdS nanorods, displaying that introduction of CoO can effectively inhibit the recombination of electron-hole pairs and improve the transport rate of the photocarriers. Time-resolved PL decay spectra was measured (Fig. 3c) and the corresponding decay parameters are listed in Table S2 in ESI†. Compared with CdS nanorods, an increase in the PL lifetime of the CdS/CoO-1h heterostructures again confirms the high migration and separation efficiency of photocarriers.[43] The density of charge carrier (N_d) is important for the photocatalysts and is calculated from Mott–Schottky analysis (Fig. 3d) to further probe the charge-transfer process. The carrier density of the CdS/CoO-1h heterostructures is 3.2×10^{17} cm^{-3}, remarkably higher than that of CdS nanorods (2.4×10^{16} cm^{-3}). This higher carrier density distinctly reveals that introduction of CoO can suppresses the recombination of electron-hole pairs in CdS nanorods. Also, the CdS/CoO-1h heterostructures show a higher photocurrent density than CdS (Fig. 4a) and a smaller diameter of the semicircles in electrochemical impedance spectroscopy (EIS) under either light or dark condition (Fig. 4b), indicating that the separation of photoexcited charge carries can be strengthened through constructing heterojunctions, which may boost the photocatalytic activity for hydrogen evolution.[50, 51]

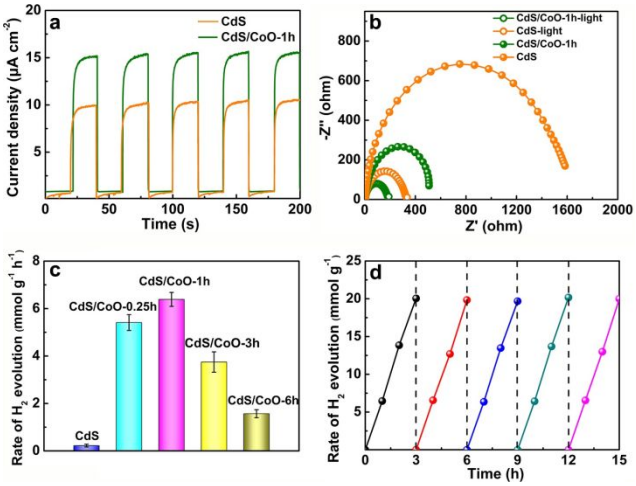

Fig. 4 (a) Photocurrent response of the CdS nanorods and CdS/CoO-1h heterostructures, (b) Nyquist plots of electrochemical impedance spectroscopy of the CdS nanorods and CdS/CoO-1h heterostructures under dark and light conditions, (c) photocatalytic hydrogen evolution activities of different catalysts, and (d) recycled hydrogen evolution property of CdS/CoO-1h heterostructures for a time period of 15 h.

The photocatalytic hydrogen evolution tests were conducted under visible light (>420 nm) irradiation. As shown in Fig. 4c, significant improvement in hydrogen evolution rate is established after coupling CoO with CdS. The pristine CdS nanorods exhibit a hydrogen production rate of 0.18 mmol g^{-1} h^{-1}. The CdS/CoO-1h heterostructures can reach a maximum rate of 6.45 mmol g^{-1} h^{-1}, ~36 times higher than that of pure CdS and is much higher than CdS/Pt (0.98 mmol g^{-1} h^{-1}) at the same loading of cocatalyst (Fig. S19 in ESI†), implying that CoO works much better than noble metal Pt as a co-catalyst in this system. Impressively, this hydrogen evolution efficiency is much better than that of many reported works (Table S3 in ESI†).[8, 13, 52] The oberserved enhanced photocatalytic activity might be rationalized by the fact that with the formed Co-S bonds between CoO and CdS in the CdS/CoO heterostructures, the photogenerated carriers can be transferred more efficiently, and thus the lifetime of charge carriers is greatly increased. Besides, the CoO nanoparticles here are very small in size, which not only serve as an important component of the heterostructures, but also provide a large number of active sites, so the photocatalytic hydrogen production rate can be increased significantly by adjusting the content of CoO in the

CdS/CoO heterostructures. Moreover, the AQY under different wavelenghs was measured to further characterize the efficiency of photocatalytic hydrogen evolution for CdS/CoO heterostructures, which is 40.64% at 420 nm and 17.45% at 500 nm (Fig. S20 in ESI†). The CdS/CoO-1h heterostructures can also provide stable photocatalytic hydrogen evolution (Fig. 4d), with no obvious activity loss after five cycles. The SEM, TEM, XRD and XPS measurements of the CdS/CoO-1h heterostructures collected after five cycles suggest neither chemical composition change nor structural collapse (Fig. S21-23 in ESI†), demonstrating their good chemical stability during the photocatalytic process and that introduction of CoO also improves the photocorrosion issue of CdS materials.

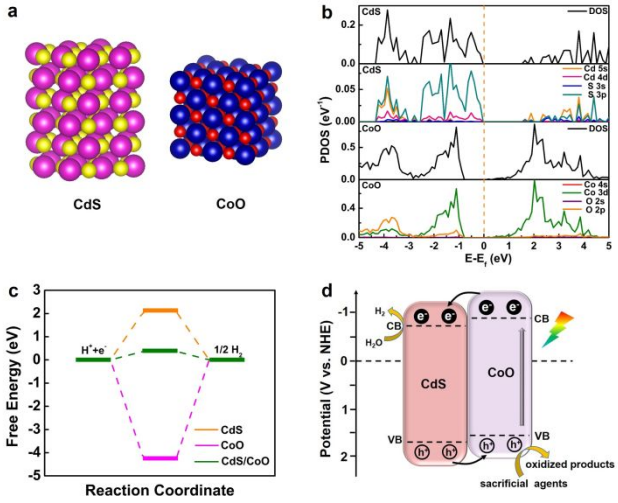

Fig. 5 (a) Optimized geometry structures of CdS and CoO, (b) the corresponding density of state plots of CdS and CoO (the dashed line represents the Fermi level), (c) free energy diagram for hydrogen adsorption on CdS, CoO and CdS/CoO, and (d) schematic illustration of the possible charge transfer process in the CdS/CoO heterostructures.

In order to better understand the real active sites, density functional theory (DFT) calculations were applied to study the density of states (DOS) and hydrogen adsorption free energy ΔG_H (see Computational Methods for details) of CdS, CoO and CdS/CoO. The optimized geometry structures of CdS and CoO are shown in Fig. 5a. It is revealed that the valence band (VB) top of CdS consists of S 3p and Cd 4d states, and the CB bottom mainly consists of S 3p state (Fig. 5b). For CoO, Co 3d and O 2p states contribute to the VB top, and the CB bottom consists of Co 3d. Notably, VB top of CdS is more positive than that of CoO, an indication that CdS has a relatively stronger reducing ability, and CoO will act as the oxidation region,[43] which again proves that the electron density of CdS is increased through the decoration of CoO nanoparticles. ΔG_H has been used as an indicator to evaluate the activity of hydrogen evolution reaction of investigated catalysts.[52] It is not conducive to hydrogen desorption if the interaction between the catalyst and hydrogen is too strong, and in turn, if hydrogen cannot be adsorbed on the catalyst, the hydrogen formation requires additional energy.[13, 53] Our calculation results show that the ΔG_H value for CdS/CoO heterostructures is close to zero when compared to that of bare CdS and CoO, suggesting the excellent catalytic activity for hydrogen evolution on the fabricated heterostructures (Fig. 5c and S24 in ESI†). Consequently, the charge transfer route in the CdS/CoO heterostructures under visible-light irradiation can be illustrated in Fig. 5d. The optical bandgaps for CdS and CoO are ~2.41 and ~2.40 eV, and the Mott-Schottky plots indicate that the estimated CB potential of CdS (-0.74 V) lies below that of CoO (-0.80 V) (Fig. S25 in ESI†). Therefore, electrons are excited from the VB to the CB of CoO nanoparticles, which then transfer to the CB of CdS nanorods rapidly. Then, hydrogen production mostly originates from the CdS surface, and CoO plays a significant role as an efficient cocatalyst. It is believed that the formed Co-S bonds can effectively facilitate the migration of photogenerated charge carriers in the CdS/CoO heterostructures and thus the photocatalytic hydrogen evolution rate can be significantly enhanced.

Conclusions

In summary, we demontrate that the photocatalytic hydrogen evolution performance of CdS nanorods can be dramatically enhaned by the introduction of highly dispersed ultrafine CoO nanoparticles as a novel and efficient non-precious cocatalyst. It is explored that production of hierarchical ultrathin $Co(OH)_2$ nanosheets through mimicking MOFs synthesis can be an effective approach to preparing ultrafine CoO nanoparticles. Due to the formation of Co-S bonds between CoO and CdS, migration and separation of photogenerated charge carriers are significantly facilitated in the as-prepared CdS/CoO heterostructures. As a consequence, the CdS/CoO-1h heterostructures show a highest hydrogen evolution rate of 6.45 mmol g^{-1} h^{-1} and a promising recycling stability without activity decay for 15 h in the absence of precious co-catalyst, which is 36 times higher than that of bare CdS nanorods and better than most reported CdS-based photocatalysts. This work provides a facile strategy for the synthesis and application of untralfine CoO nanoparticles as an alternative cocatalyst to Pt in photocatalytic water splitting for hydrogen production.

Conflicts of interest

There are no conflicts to declare.

Acknowledgements

We thank the financial support from the National Natural Science Foundation of China (21471039, 21571043, 21671047, and 21871065), and Natural Science Foundation of Heilongjiang Province (B2015001). This research used resources of the 23-ID-2 (IOS) beamline of the National Synchrotron Light Source II, a U.S. Department of Energy (DOE) Office of Science User Facility operated for the DOE Office of Science by Brookhaven National Laboratory under Contract No. DE-SC0012704.

Notes and references

1. X. Chen, L. Liu, P. Y. Yu and S. S. Mao, *Science*, 2011, **331**, 746-750.
2. J. Liu, Y. Liu, N. Liu, Y. Han, X. Zhang, H. Huang, Y. Lifshitz, S. T. Lee, J. Zhong and Z. Kang, *Science*, 2015, **347**, 970-974.
3. S. Wang, B. Y. Guan and X. W. D. Lou, *J. Am. Chem. Soc.*, 2018, **140**, 5037-5040.
4. P. Zhang and X. W. D. Lou, *Adv. Mater.*, 2019, 1900281.
5. M. Lan, R. M. Guo, Y. Dou, J. Zhou, A. Zhou and J. R. Li, *Nano Energy*, 2017, **33**, 238-246.
6. G. Liu, Y. Zhao, C. Sun, F. Li, G. Q. Lu and H. M. Cheng, *Angew. Chem. Int. Ed.*, 2008, **47**, 4516-4520.
7. S. Wang, B. Y. Guan, X. Wang and X. W. D. Lou, *J. Am. Chem. Soc.*, 2018, **140**, 15145-15148.
8. L. Shang, B. Tong, H. Yu, G. I. N. Waterhouse, C. Zhou, Y. Zhao, M. Tahir, L. Z. Wu, C. H. Tung and T. Zhang, *Adv. Energy Mater.*, 2016, **6**, 1501241.
9. X. Li, J. Yu and M. Jaroniec, *Chem. Soc. Rev.*, 2016, **45**, 2603-2636.
10. J. Liu, K. Chen, G.-M. Pan, Z.-J. Luo, Y. Xie, Y.-Y. Li, Y.-J. Lin, Z.-H. Hao, L. Zhou, S.-J. Ding and Q.-Q. Wang, *Nanoscale*, 2018, **10**, 19586-19594.
11. Y. Luo, B. Deng, Y. Pu, A. Liu, J. Wang, K. Ma, F. Gao, B. Gao, W. Zou and L. Dong, *Appl. Catal. B-Environ.*, 2019, **247**, 1-9.
12. Y. Luo, J. Wang, S. Yu, Y. Cao, K. Ma, Y. Pu, W. Zou, C. Tang, F. Gao and L. Dong, *J. Mater. Research*, 2018, **33**, 1268-1278.
13. G. Zhao, Y. Sun, W. Zhou, X. Wang, K. Chang, G. Liu, H. Liu, T. Kako and J. Ye, *Adv. Mater.*, 2017, **29**, 1703258.
14. C. Ding, J. Shi, Z. Wang and C. Li, *ACS Catal.*, 2017, **7**, 675-688.
15. S. Wang, B. Y. Guan, Y. Lu and X. W. D. Lou, *J. Am. Chem. Soc.*, 2017, **139**, 17305-17308.
16. J. Peng, J. Xu, Z. Wang, Z. Ding and S. Wang, *Phys. Chem. Chem. Phys.*, 2017, **19**, 25919-25926.
17. P. Zhou, F. Lv, N. Li, Y. Zhang, Z. Mu, Y. Tang, J. Lai, Y. Chao, M. Luo, F. Lin, J. Zhou, D. Su and S. Guo, *Nano Energy*, 2019, **56**, 127-137.
18. R. Su, N. Dimitratos, J. Liu, E. Carter, S. Althahban, X. Wang, Y. Shen, S. Wendt, X. Wen, J. W. Niemantsverdriet, B. B. Iversen, C. J. Kiely, G. J. Hutchings and F. Besenbacher, *ACS Catal.*, 2016, **6**, 4239-4247.
19. S. Ida, K. Sato, T. Nagata, H. Hagiwara, M. Watanabe, N. Kim, Y. Shiota, M. Koinuma, S. Takenaka, T. Sakai, E. Ertekin and T. Ishihara, *Angew. Chem. Int. Ed.*, 2018, **57**, 9073-9077.
20. Y. Liu, B. Zhang, L. Luo, X. Chen, Z. Wang, E. Wu, D. Su and W. Huang, *Angew. Chem. Int. Ed.*, 2015, **54**, 15260-15265.
21. F. Li, Y. Hou, Z. Yu, L. Qian, L. Sun, J. Huang, Q. Ran, R. Jiang, Q. Sun and H. Zhang, *Nanoscale*, 2019, **11**, 10884-10895.
22. Y. Zhang, Z. Peng, S. Guan and X. Fu, *Appl. Catal. B-Environ.*, 2018, **224**, 1000-1008.
23. Z. Li, J. Hou, B. Zhang, S. Cao, Y. Wu, Z. Gao, X. Nie and L. Sun, *Nano Energy*, 2019, **59**, 537-544.
24. R. Li, H. Han, F. Zhang, D. Wang and C. Li, *Energy Environ. Sci.*, 2014, **7**, 1369-1376.
25. T. Su, Z. D. Hood, M. Naguib, L. Bai, S. Luo, C. M. Rouleau, I. N. Ivanov, H. Ji, Z. Qin and Z. Wu, *Nanoscale*, 2019, **11**, 8138-8149.
26. Y. Liu, S. Ding, Y. Shi, X. Liu, Z. Wu, Q. Jiang, T. Zhou, N. Liu and J. Hu, *Appl. Catal. B-Environ.*, 2018, **234**, 109-116.
27. Z. Mao, J. Chen, Y. Yang, D. Wang, L. Bie and B. D. Fahlman, *ACS Appl. Mater. Interfaces*, 2017, **9**, 12427-12435.
28. L. Liao, Q. Zhang, Z. Su, Z. Zhao, Y. Wang, Y. Li, X. Lu, D. Wei, G. Feng, Q. Yu, X. Cai, J. Zhao, Z. Ren, H. Fang, F. Robles-Hernandez, S. Baldelli and J. Bao, *Nat. Nanotech.*, 2014, **9**, 69-73.
29. F. Guo, W. Shi, C. Zhu, H. Li and Z. Kang, *Appl. Catal. B-Environ.*, 2018, **226**, 412-420.
30. D. Wang, Z. P. Liu and W. M. Yang, *ACS Catal.*, 2018, **8**, 7270-7278.
31. S. Hong, D. P. Kumar, E. H. Kim, H. Park, M. Gopannagari, D. A. Reddy and T. K. Kim, *J. Mater. Chem. A*, 2017, **5**, 20851-20859.
32. J. Chu, X. Han, Z. Yu, Y. Du, B. Song and P. Xu, *ACS Appl. Mater. Interfaces*, 2018, **10**, 20404-20411.
33. S. Ouyang, H. Tong, N. Umezawa, J. Cao, P. Li, Y. Bi, Y. Zhang and J. Ye, *J. Am. Chem. Soc.*, 2012, **134**, 1974-1977.
34. G. Kresse and J. Furthmuller, *Phys. Rev. B*, 1996, **54**, 11169-11186.
35. G. Kresse and D. Joubert, *Phys. Rev. B*, 1999, **59**, 1758-1775.
36. J. P. Perdew, M. Emzerhof and K. Burke, *J. Chem. Phys.*, 1996, **105**, 9982-9985.
37. J. Xu, X. Li, Z. Ju, Y. Sun, X. Jiao, J. Wu, C. Wang, W. Yan, H. Ju, J. Zhu and Y. Xie, *Angew. Chem. Int. Ed.*, 2018, **58**, 1-6.
38. H. Hu, L. Han, M. Yu, Z. Wang and X. W. Lou, *Energy Environ. Sci*, 2016, **9**, 107-111.
39. D. Gallant, M. Pezolet and S. Simard, *J. Phys. Chem. B*, 2006, **110**, 6871-6880.
40. W. Shi, F. Guo, H. Wang, S. Guo, H. Li, Y. Zhou, C. Zhu, Y. Liu, H. Huang, B. Mao, Y. Liu and Z. Kang, *ACS Appl. Mater. Interfaces*, 2017, **9**, 20585-20593.
41. C. W. Kung, H. W. Chen, C. Y. Lin, K. C. Huang, R. Vittal and K. C. Ho, *ACS Nano*, 2012, **6**, 7016-7025.
42. B. Liu, L. Ma, L. C. Ning, C. J. Zhang, G. P. Han, C. J. Pei, H. Zhao, S. Z. Liu and H. Q. Yang, *ACS Appl. Mater. Interfaces*, 2015, **7**, 6109-6117.
43. Y. Chao, P. Zhou, N. Li, J. Lai, Y. Yang, Y. Zhang, Y. Tang, W. Yang, Y. Du, D. Su, Y. Tan and S. Guo, *Adv. Mater.*, 2018, **31**, 1807226.
44. J. Ran, J. Qu, H. Zhang, T. Wen, H. Wang, S. Chen, L. Song, X. Zhang, L. Jing, R. Zheng and S. Z. Qiao, *Adv. Energy Mater.*, 2019, **9,** 1803402.
45. H. Zhang, P. Zhang, M. Qiu, J. Dong, Y. Zhang and X. W. D. Lou, *Adv. Mater.*, 2018, **31**, 1804883.
46. M. Zhu, S. Kim, L. Mao, M. Fujitsuka, J. Zhang, X. Wang and T. Majima, *J. Am. Chem. Soc.*, 2017, **139**, 13234-13242.
47. A. M. Hibberd, H. Q. Doan, E. N. Glass, F. M. F. de Groot, C. L. Hill and T. Cuk, *J. Phys. Chem. C*, 2015, **119**, 4173-4179.
48. W. S. Yoon, K. B. Kim, M. G. Kim, M. K. Lee, H. J. Shin and J. M. Lee, *J. Electrochem. Soc.*, 2002, **149**, 1305-1309.
49. L. Zhou, C. Zhao, B. Giri, P. Allen, X. Xu, H. Joshi, Y. Fan, L. V. Titova and P. M. Rao, *Nano Lett*, 2016, **16**, 3463-3474.
50. Y. Huang, Y. Lu, Y. Lin, Y. Mao, G. Ouyang, H. Liu, S. Zhang and Y. Tong, *J. Mater. Chem. A*, 2018, **6**, 24740-24747.
51. S. Ma, Y. Deng, J. Xie, K. He, W. Liu, X. Chen and X. Li, *Appl. Catal. B-Environ.*, 2018, **227**, 218-228.
52. B. Song, K. Li, Y. Yin, T. Wu, L. Dang, M. Caban-Acevedo, J. Han, T. Gao, X. Wang, Z. Zhang, J. R. Schmidt, P. Xu and S. Jin, *ACS Catal.*, 2017, **7**, 8549-8557.

53. J. K. Norskov, T. Bligaard, A. Logadottir, J. R. Kitchin, J. G. Chen and S. Pandelov, *J. Electrochem. Soc.*, 2005, **152**, 23-26.

Graphical Abstract

Ultrafine CoO nanoparticles as an efficient cocatalyst for enhanced photocatalytic hydrogen evolution

Jiayu Chu,[a] Guoji Sun,[b] Xijiang Han,*[a] Xin Chen,[c] Jiajun Wang,[a] Wen Hu,[d] Iradwikanari Waluyo,[d] Adrian Hunt,[d] Yunchen Du,[a] Bo Song,*[e] and Ping Xu*[a]

[a] MIIT Key Laboratory of Critical Materials Technology for New Energy Conversion and Storage, School of Chemistry and Chemical Engineering, Harbin Institute of Technology, Harbin 150001, China.

[b] State Key Laboratory of Advanced Welding and Joining, Harbin Institute of Technology, Shenzhen Graduate School, Shenzhen 518055, China.

[c] School of Advanced Materials, Peking University, Shenzhen Graduate School, Shenzhen 518055, China.

[d] National Synchrotron Light Source II, Brookhaven National Laboratory, Upton, NY 11973, USA.

[e] Academy of Fundamental and Interdisciplinary Sciences, Harbin Institute of Technology, Harbin 150001, China.

*Corresponding authors. E-mail: pxu@hit.edu.cn (P.X.); hanxijiang@hit.edu.cn (X.H.); songbo@hit.edu.cn (B.S.).

Highly dispersed ultrafine CoO nanoparticles, as a novel and efficient cocatalyst, can dramatically enhance the photocatalytic hydrogen evolution rate of CdS nanorods in the visible-light region.